Predictive masking of an artificial scotoma is associated with a system-wide reconfiguration of neural populations in the human visual cortex

Carvalho, Joana; Renken, Remco J; Cornelissen, Frans W

Published in:
Neuroimage

DOI:
10.1016/j.neuroimage.2021.118690

Publication date:
2021

NeuroImage 245 (2021) 118690

Contents lists available at ScienceDirect

NeuroImage

journal homepage: www.elsevier.com/locate/neuroimage

Predictive masking of an artificial scotoma is associated with a system-wide reconfiguration of neural populations in the human visual cortex

Joana Carvalho[a,b,*], Remco J. Renken[c], Frans W. Cornelissen[a]

[a] Laboratory of Experimental Ophthalmology, University Medical Center Groningen, University of Groningen, Groningen, The Netherlands
[b] Laboratory of Preclinical MRI, Champalimaud Centre for the Unknown, Avenida de Brasília, Lisbon, Portugal 1400-038
[c] Cognitive Neuroscience Center, University Medical Center Groningen, University of Groningen, Groningen, The Netherlands

ARTICLE INFO

Keywords:
Prediction
Masking
Population receptive field
Connective field
Reorganization
Artificial scotoma
fMRI

ABSTRACT

The visual brain has the remarkable capacity to complete our percept of the world even when the information extracted from the visual scene is incomplete. This ability to predict missing information based on information from spatially adjacent regions is an intriguing attribute of healthy vision. Yet, it gains particular significance when it masks the perceptual consequences of a retinal lesion, leaving patients unaware of their partial loss of vision and ultimately delaying diagnosis and treatment. At present, our understanding of the neural basis of this masking process is limited which hinders both quantitative modeling as well as translational application. To overcome this, we asked the participants to view visual stimuli with and without superimposed artificial scotoma (AS). We used fMRI to record the associated cortical activity and applied model-based analyzes to track changes in cortical population receptive fields and connectivity in response to the introduction of the AS. We found that throughout the visual field and cortical hierarchy, pRFs shifted their preferred position towards the AS border. Moreover, extrastriate areas biased their sampling of V1 towards sections outside the AS projection zone, thereby effectively masking the AS with signals from spared portions of the visual field. We speculate that the signals that drive these system-wide population modifications originate in extrastriate visual areas and, through feedback, also reconfigure the neural populations in the earlier visual areas.

1. Introduction

Predictive masking (PM) can be considered as a manifestation of the visual system trying to predict perceptual events. PM plays a prominent role in healthy perception, e.g. evident from the masking of the blind spot and from many visual illusions in which color, brightness, or textures spread into and mask neighbouring regions of the visual field (Komatsu, 2006; Pessoa and De Weerd, 2003). Consequently, the process is sometimes also referred to by this behavioral manifestation as “filling-in”. PM is a highly heterogeneous phenomenon, which can be instantaneous, i.e. blind spot, or requiring a prolonged fixation before it occurs, i.e. artificial scotoma (AS) (Weil and Rees, 2011). Despite this temporal mismatch required to stabilize an AS on the retina, an AS overlaid on a dynamic noise pattern is used as an useful model that mimics the short-term effects of natural scotomas (Dreher et al., 2001; Kapadia et al., 1994; Parks and Corballis, 2012; Ramachandran et al., 199 3). Long term PM, which may share similar underlying mechanisms as short-term PM, lies at the basis of the masking of retinal lesions, which often leaves patients unaware of their partial loss of vision. Consequently, such masking results in delayed diagnosis and treatment of the disease underlying the lesions, i.e. glaucoma (Hoste, 2003; Smith et al., 2012; Spillmann and Kurtenbach, 1992).

Despite the scientific and clinical relevance of understanding PM, its underlying neural mechanisms are poorly understood. In particular, the top-down versus bottom-up neural origin of PM has been strongly debated (Binda et al., 2013; Calford, 2002b; DeAngelis et al., 1995; De Weerd et al., 1995; Dilks et al., 2009, 2007; Gilbert and Wiesel, 1992; Masuda et al., 2008; Smirnakis et al., 2005). Bottom-up theories suggest that the neural mechanism of PM has its origin at the early visual cortex and that effects are propagated to extrastriate areas. This bottom-up view is supported by studies of the neural consequences of permanent retinal lesions, which have shown receptive field (RF) expansion and shifts in RF preferred position towards spared portions of the visual field (Baker et al., 2005; Calford, 2002a; Dilks et al., 2007; Gilbert and Wiesel, 1992; Kapadia et al., 1994; Pettet and Gilbert, 1992; Tailby and Metha, 2004). However, such RF changes also occur following simulated scotomas, thus suggesting that these changes may not result from structural plasticity (Baseler et al., 2011; Haak et al., 2012;

PM, Predictive Masking; AS, Artificial Scotoma; RF, Receptive Field; SPZ, Scotoma Projection Zone.

* Correspondence author at: Laboratory of Preclinical MRI, Champalimaud Centre for the Unknown, Avenida de Brasília, Lisbon 1400-038, Portugal.
E-mail address: joana.carvalho@research.fchampalimaud.org (J. Carvalho).

https://doi.org/10.1016/j.neuroimage.2021.118690.
Received 20 July 2021; Received in revised form 19 October 2021; Accepted 28 October 2021
Available online 7 November 2021.

Papanikolaou et al., 2015). Consistent with a top-down mechanism, the observed RF changes may be an indirect consequence of modulating the responsiveness of neurons in the scotoma projection zone (SPZ). These top-down mechanisms act through multiple forms to convey information from higher-order to antecedent cortical areas, in particular: gain adjustments that reduce the feedforward information (Das and Gilbert, 1995; Parks and Corballis, 2012; Tremere et al., 2003; Weil et al., 2008); downregulation of inhibition (De Weerd et al., 1995; Smirnakis et al., 2005; DeAngelis et al., 1995; Mendola et al., 2006); feedback from higher-order areas with large RFs (Angelucci et al., 2002; De Weerd et al., 2006; Fiorani Júnior et al., 1992; Harrison et al., 2007); feature-based-attention which shifts the RF centers toward the focus of attention, (Klein et al., 2014; Womelsdorf et al., 2008) and predictive coding strategy, where higher-levels in the cortical hierarchy make predictions about lower-level activity (Rao and Ballard, 1999; Spratling, 2010). PM can also be considered as the perceptual manifestation of neural adaptation. In contrast to RF changes underlying cortical remapping, adaptation is very fast and does not rely on structural changes in the visual neural circuitry but rather on functional interactions, such as inhibition (Clifford et al., 2007; Haak et al., 2015; Kohn, 2007; Wandell and Smirnakis, 2009). Functional changes resulting from adaptation are also referred to as short-term plasticity.

The observed changes in RF properties led to the controversial hypothesis that PM is explained by neurons modifying their RF properties (Pettet and Gilbert, 1992). Nevertheless, the precise neural basis of PM remains unknown. In addition, previous studies assumed that PM is driven by local mechanisms restricted to the SPZ. However, if PM is a perceptual consequence of functional changes, i.e. gain, we would expect neurophysiological modifications to occur both inside and outside the SPZ and throughout the visual hierarchy. In the present study, we tested the hypothesis that PM involves a visual system-wide reconfiguration of RFs and their connectivity. Specifically, we expect that in the cortical region responsible for PM, the neural mechanisms within the SPZ should show a decreased reliance on information coming from within the AS and a simultaneously increased reliance on information coming from outside of it. Confirming this hypothesis will lead to more accurate models of visual perception and improve diagnostic methods for patients with visual field defects.

To test our hypothesis, we used functional MRI in combination with biologically-inspired neural population modeling to track changes in RF properties and cortical connectivity following the introduction of an AS into the visual field of human participants (mimicking a retinal lesion). We modeled the observed changes in pRF position using a gain field model and we examined how cortical connections between visual areas and locations (inside and outside ASPZ) changed in response to the AS.

2. Materials and methods

2.1. Functional imaging

Retinotopic mapping was performed under three different stimulus conditions: a conventional retinotopy stimulus based on luminance contrast (LCR) used for delineating visual areas, an artificial scotoma stimulus (AS^+) and a control stimulus identical to AS^+ but without the artificial scotoma (AS^-), Fig. 1. The stimuli used in the two AS conditions were designed to stimulate the low spatial frequency selective neurons predominantly. The low spatial frequency carries coarse information about the visual scene and it is presumably encoded mainly by neurons with large RFs (Chen et al., 2009; Enroth-Cugell and Freeman, 1987). This is expected to facilitate PM.

Prior to performing imaging, we performed pilot psychophysical experiments to optimize the stimulus characteristics to yield the most stable perceptual masking, which included using low spatial frequency dynamic noise background, placing the scotomas peripherally, using multiple relatively small scotomas and a continuously moving bar. Specifically, in a psychophysical experiment, we tested more in-depth whether a dynamic noise background composed of low spatial frequencies facilitates PM. We found that low spatial frequencies (0–2 cpd) drive a faster perceptual filling-in effect than higher spatial frequencies, i.e. 2–4 cpd, Fig. S1.

2.2. Participants and ethics statement

Seven participants (3 females; average age: 28; age-range: 26–32) with normal or corrected-to-normal vision were included in the study. The participants indicated that they understood the instructions. Prior to participation, participants signed an informed consent form. Our study was approved by the Medical Ethical Review Board of the University Medical Center of Groningen, and conducted in accordance with the Declaration of Helsinki. The data is available at XNAT central under the project ID: fMRI_PM.

2.3. Data acquisition

Stimuli were presented on an MR compatible display screen (BOLDscreen 24 LCD; Cambridge Research Systems, Cambridge, UK). The screen was located at the head-end of the MRI scanner. Participants viewed the screen through a tilted mirror attached to the head coil. Distance from the participant's eyes to the display (measured through the mirror) was 120 cm. Screen size was 22 × 14 deg. The maximum stimulus radius was 7 deg of visual angle. Visual stimuli were created using MATLAB (Mathworks, Natick, MA, USA) and the Psychtoolbox (Brainard, 1997; Pelli, 1997).

2.4. Stimuli

2.4.1. Luminance-contrast defined retinotopy (LCR)

LCR consists of a drifting bar aperture defined by high-contrast flickering texture (Dumoulin and Wandell, 2008). The bar aperture, i.e. alternating rows of high-contrast luminance checks drifting in opposite directions, moved in 8 different directions (four bar orientations: horizontal, vertical and the two diagonal orientations), with two opposite drift directions for each orientation (Fig. 1A). The bar moved across the screen in 16 equally spaced steps each lasting 1 TR. The bar contrast, width and spatial frequency were 100%, 1.75° of visual angle and 0.5 cycles per degree, respectively. After 24 steps (one pass and a half), 12 s of a blank full screen stimulus at mean luminance was presented.

2.4.2. Artificial scotoma (AS) conditions

The stimuli used in the two AS conditions were adapted from the LCR stimulus. More specifically, the bar and background could be distinguished from each other only on the basis of their spatial frequency (Fig. 1B). The AS^- condition served as the control condition for the AS^+condition that contained the actual scotoma. The bar's movement directions and orientations matched those of the LCR condition. The width of the bar aperture was 3°. The bar content was dynamic white-noise band pass filtered at frequencies from 0 to 2 cycles per degree (cpd). The background noise consisted of a dynamic white spatial frequency band passed from 2 to 4 cpd. The long edges of the bar were smoothed using an exponential mask. The formula for this mask was: $= e^{-\frac{r^f}{2}}$, where r is the distance to the center-line of the bar, and f the mask factor. The value of f was fixed at 4. The bar moved continuously at a speed of 0.46 deg/sec. This continuous movement of the bar aperture is essential for the PM of the AS. Note that during all 3 conditions (LCR, AS^- and AS^+) the bar swiped the visual field in one direction during 24 s. The AS^- condition was used to define a baseline preferred position and size of the pRF for each voxel.

The AS^+ condition was similar to AS^- (with equal bar aperture size, movement and spatial frequency). Four ASs were superimposed on the dynamic noise background (see Fig. 1C). The scotomas were centered at each quarter field at 4.5 deg of eccentricity. Each AS consisted of

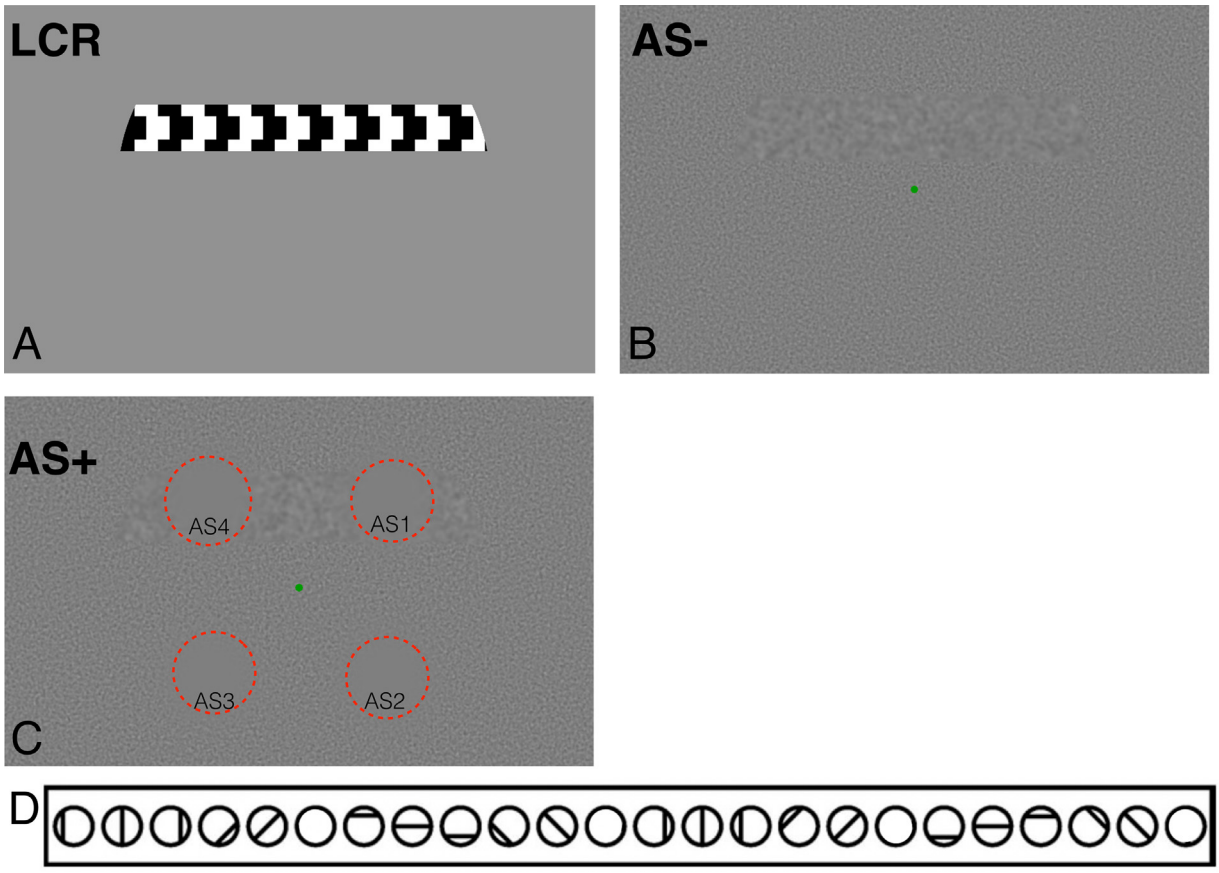

Fig. 1. Example of the stimuli used to obtain pRF parameter estimates. A: LCR; B: AS^{-}, C: AS^{+}, for visualization purposes the four AS are outlined with a dashed red line and the AS are numbered. NB: during the experiment, the red dashed lines and the labels of the AS were not presented to the participants. D: Scheme of the bar movements: four orientations in two opposing directions (For interpretation of the references to color in this figure legend, the reader is referred to the web version of this article.).

2.5 deg radius disk tapered by an exponential mask at the edges, similar to the masking of the bar: $= e^{-\frac{r^f}{2}}$, where, r is the distance from the center of the scotoma and f is fixed at a value of four, as before. Preceding each run was a one-minute adaptation period during which the participants viewed only the background with the AS superimposed while performing the fixation attentional task. In psychophysical experiments, performed prior to the fMRI scans, we determined that this period was sufficient to induce filling-in. Importantly when the moving bar moved over the AS the participants perceived the bar as complete, meaning that the participants do not fill-in only to background but also to the new spatial frequency of the bar.

2.4.3. Attentional task

During retinotopic mapping, participants were required to perform a fixation task in which they had to press a button each time the fixation point turned from green to red. The fixation tasks allow us to probe if the participants are fixating correctly and focused. The average performance on this task was above 86% for all the conditions (LCR: 90.9% ± 6.8; AS-: 86.0% ± 8.7; AS+: 87.7% ±3.4). One-way repeated measures ANOVA showed no significant difference between the attention task performance between the conditions AS^{+} and AS^{-} ($p = 0.6341$).

2.4.4. MRI scanning and preprocessing

Scanning was carried out on a 3 Tesla Siemens Prisma MR-scanner using a 64-channel receiving head coil. A T1-weighted scan (voxel size, 1 mm^3; matrix size, 256 × 256 × 256) covering the whole brain was recorded to chart each participant's cortical anatomy. The functional scans were collected using standard EPI sequence (TR, 1500 ms; TE, 30 ms; voxel size, 3 mm^3, flip angle 80; matrix size, 84 × 84 × 24). Slices were oriented to be approximately parallel to the calcarine sulcus. For the retinotopic scans LCR and AS^{-} a single run consisted of 136 functional images (duration of 204 s) and for AS^{+}a single run consisted of 168 functional images (252 s).

The T1-weighted whole-brain anatomical images were reoriented in AC-PC space. The resulting anatomical image was automatically segmented using Freesurfer (Dale et al., 1999) and subsequently edited manually. The cortical surface was reconstructed at the gray/white matter boundary and rendered as a smoothed 3D mesh (Wandell et al., 2000).

The functional scans were analyzed in the mrVista software package for MATLAB (available at http://white.stanford.edu/software). Head movements between and within functional scans were corrected (Nestares and Heeger, 2000). The functional scans were averaged and co-registered to the anatomical scan and interpolated to a 1 mm isotropic resolution. Drift correction was performed by detrending the BOLD time series with a discrete cosine transform filter with a cutoff frequency of 0.001 Hz. To avoid possible saturation effects, initial images were discarded for the LCR and AS^{-} (8 TRs). For the AS^{+} condition the 40 initial images were discarded (40 TRs). Note that the full 60 s adaptation period was removed for the AS^{+}.

2.4.5. Experimental procedure

Each participant completed two fMRI sessions of approximately 1.5 h. In the first fMRI session, 5 participants were subjected to the

anatomical scan and LCR, and they performed the AS$^-$ experiment (6 runs, 3.4 min each). In the second fMRI session, the AS$^+$ experiment (6 runs, 4.2 min each) were performed. To mitigate the possibility that differences between conditions (AS$^+$ and AS$^-$) would result from the acquisition in different sessions, these were performed for 2 participants (S06 and S07) in the same session.

2.4.6. Behavioral experiment

Although PM is linked to perceptual filling-in, we opted to not quantify perceptual filling-in during our experiments. This is because such a perceptual task could interfere with the attention task and increase the chance of participants unintentionally making small eye-movements in the direction of the AS, thereby actually decreasing filling-in magnitude. Therefore, we performed psychophysical tests outside of the scanner and prior to the neuroimaging study, primarily to determine the time required that ensures that complete filling-in of the AS would occur.

Six of the seven participants included in the functional imaging study participated in this psychophysical experiment. The stimulus background with four AS was identical to that used in the fMRI experiment. The participant's task was to fixate in the center of the screen (represented by a white dot – 0.15 deg radius) and press a button when the background was perceived as uniform (indicating that the AS had been filled in). During this filling-in experiment, participants' fixation maintenance was verified through eye movement recording. Filling-in time corresponded to the time interval since the start of the presentation of the scotomas until a button press was recorded. Per participant, four repetitions (trials) were performed. Between two consecutive trials there was a period of 15 s during which a uniform gray background was shown in order to prevent carryover. To verify that stable filling-in of the AS would also occur during pRF mapping, additional trials with a moving bar were performed. All participants reported stable and continuous filling-in of the AS both to the background and to the mapping bar.

During the behavioral experiment, the stimuli were presented on a 22-inch CRT screen (LaCie) with a resolution of 1024 × 768 pixels and a refresh rate of 120 Hz. MATLAB (MathWorks) using the Psychophysics Toolbox (Brainard, 1997; Pelli, 1997) and EyeLink Toolbox extensions (Cornelissen et al., 2002) was used to program the stimuli, their presentation and to record eye movements and observers' responses. Eye movements were recorded at 500 Hz with an EyeLink 1000 (SR Research, Kanata, Ontario, Canada) infrared eye tracker. We used the EyeLink's built-in nine-point calibration procedure. A chin and forehead rest was used to reduce the head movement of the observers.

2.4.7. Visual field mapping: pRF modeling and micro probing

The pRF analysis was performed using both conventional pRF mapping (Dumoulin and Wandell, 2008) and Micro-Probing (MP) (Carvalho et al., 2020). In the conventional method, a 2D-Gaussian model was fitted with parameters: center (x0, y0) and size (σ - width of the Gaussian) for each voxel. All the parameter units are in degrees of visual angle and are stimulus-referred. We used SPM's canonical Haemodynamic Response Function (HRF) model. The conventional pRF estimation was performed in volume space (one pRF model estimated per voxel) using the mrVista (VISTASOFT) MATLAB toolbox.

Using MP, a pRF profile is created by sampling the visual space with a large number of "micro-probes" (10,000), 2D-Gaussians with center (x, y) and a small size (σ = 0.01 deg). Similar to the conventional pRF model, the overlap between each probe and the stimulus is calculated and the resulting signal is convolved with the HRF. The fit between the predicted and measured voxel's response is calculated based on the likelihood, which allows the update of the variables (x,y, new probe), for the next iteration. The visual field sampling is done using Bayesian Markov Chain Monte Carlo (MCMC) approach, which results in regions of the visual space that best fit a voxel's response will be more densely sampled. By aggregating all the probes generated with their corresponding variance explained, we obtain a probe map per voxel, which reflects the pRF profile. Importantly, MP is a more data driven method, with less a priori assumptions than the conventional pRF, which allows to detect multiple pRF and shapes within a voxel. By summing the pRF profiles obtained with MP for all the voxels of a visual area, we obtained the coverage map of that area (Carvalho et al., 2021).

The functional responses to LCR, AS$^-$ and AS$^+$ were analyzed using the full field (FF) model (Fig. 2A). The AS$^+$ condition was also analyzed using the scotoma field (SF) model, which takes the presence of the scotoma into account (Fig. 2B). The analysis of the AS$^+$condition using these two models allows to control for modeling biases resulting from partial stimulation due to the presence of the AS (Binda et al., 2013). Unless otherwise specified the pRF estimates presented in the results were obtained using the SF model.

2.4.8. ROI and artificial scotoma projection zones definition

The cortical borders of visual areas were derived based on phase reversal, obtained with the conventional pRF model using the classical LCR stimulus (Fig. S7). Per observer, six visual areas (V1, V2, V3, V4, LO1 and LO2) were manually delineated on the inflated cortical surface.

Based on the pRF estimates obtained in the AS$^-$ condition, the ASPZ was defined as the voxels for which the pRF was completely contained within the AS regions of the visual field. Note that as an alternative approach, we also defined the ASPZ based on a scotoma localizer in which the AS and its background were alternately stimulated using the AS$^-$ spatial frequency pattern. The results obtained using either ASPZ definition were highly similar. Therefore, here we present the results obtained only based on the first method, and for this reason we do not describe in detail the AS localizer task.

2.4.9. Gain field model

The influence of the AS on the pRF's preferred position and size was modeled as a gain field (GF), i.e., the multiplication of two Gaussian components (Klein et al., 2014; Reynolds and Heeger, 2009; Womelsdorf et al., 2008, 2006). In our study, the first Gaussian component corresponded to the pRF estimated in the AS$^-$ condition (u_{AS-},σ_{AS-}). The second Gaussian component corresponded to the GF (u_{GF},σ_{GF}) elicited by the AS: it represented the influence of the AS on the pRF's preferred position. The GF was centered on the border of the AS at the point nearest to the original pRF location (Fig. 2C). The product of these two components resulted in a third Gaussian (u_{pAS+}, σ_{pAS+}), that represented the predicted pRF in the AS$^+$ condition. Eqs. (1) and 2 show how the properties of the third Gaussian were derived.

$$u_{pAS+} = \left(\frac{u_{AS-} * \sigma_{GF}^2 + u_{GF} * \sigma_{AS-}^2}{\sigma_{GF}^2 + \sigma_{AS-}^2} \right) \quad (1)$$

$$\sigma_{pAS+} = \sqrt{\left(\frac{\sigma_{GF}^2 * \sigma_{AS-}^2}{\sigma_{GF}^2 + \sigma_{AS-}^2} \right)} \quad (2)$$

The GF size was estimated by minimizing the error between the predicted and the measured position shifts, which is the radial distance between the AS$^+$and AS$^-$. The GF size was estimated per visual area. For verification of the model's accuracy, the data was split into a training set (50% of the data) and a test set (the remaining 50% of the data). The code for the GF model is available via: https://github.com/Joana-Carvalho/Gain-field-model.

2.4.10. Connective field (CF) modeling

The CF model predicts the neuronal activity of a recording site (voxel) in a target region (e.g. in V2) given the aggregate activity in a source region (in V1) (Gravel et al., 2014; Haak et al., 2013). The fMRI response of each voxel is predicted using a 2D circular Gaussian CF model, folded to follow the cortical surface of the source region. The CF output parameters are the position and spread (size) across the source surface. Given a CF position and a size, a time-series prediction is then calculated by weighting the CF with the BOLD time series. The optimal

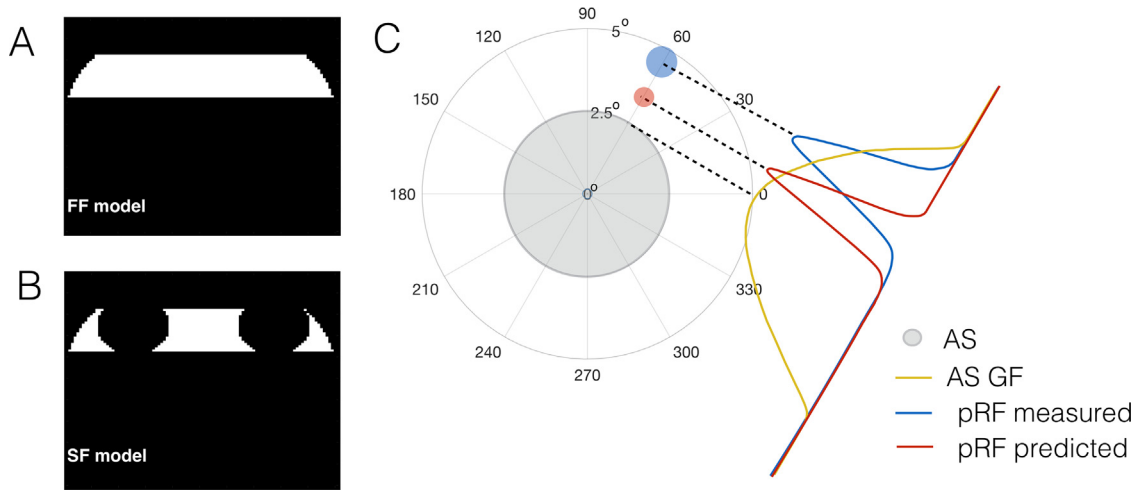

Fig. 2. Illustrations of the models of neural responses used in the analyzes. A: The full field (FF) and B: the scotoma field (SF) models used in the pRF analysis. C: AS GF model: the AS (shaded gray region) effect was modeled as the AS GF (yellow), centered at the edge of the scotoma closest to the pRF (blue). This results in a predicted pRF (red), shifted towards the scotoma. (For interpretation of the references to color in this figure legend, the reader is referred to the web version of this article.).

CF parameters are found by minimizing the residual sum of squares between the predicted and the measured time-series. In this study, only CFs with a variance explained above 30% were retained. This threshold was defined based on previous studies (Gravel et al., 2014; Haak et al., 2013). The percentage of voxels removed (mean and std across visual areas) is 51% (±19%).

The CF coverage maps were computed based on the voxel's BOLD times series. The CF coverage maps were obtained by back projecting each CF into the visual space using the pRFs for V1 obtained with AS^{-}. First, per voxel in the target region, a CF was calculated, i.e. the target voxel is expressed as the weighted (CF factor) average of the signals measured in V1 (the source region). As the pRF was known for each voxel in V1, we calculated the spatial sampling by summing all pRFs of V1 weighted by the CF factor. The total CF coverage map was calculated by summing these maps across all voxels in the target region. Finally, a group average ($n = 7$) was calculated across subjects. The code to calculate the CF coverage maps is available via: https://github.com/Joana-Carvalho/Connective-field-back-projection.

3. Statistical analysis

3.1. Population receptive field analysis

Data was thresholded by retaining the pRF models that explained at least 15% of the variance in the BOLD response in the three conditions (LCR, AS^{+}, AS^{-}). This threshold was based on previous studies (Dumoulin and Wandell, 2008; Yildirim et al., 2018). The percentage of voxels removed (mean and std across visual areas) is 32% (±7%).

For the analysis of changes in pRF properties in response to the AS, the pRF estimates of the four quadrants were collapsed onto a single quadrant. Subsequently, voxels were binned into 12 bins, each covering an eccentricity range of 1.75 deg and a polar angle range of 30° (Fig. 4B). Additionally within the ASPZ, voxels were binned into 12 bins of 30 deg of polar angle each after shifting the origin to the center of the ASPZ (Fig. 4A).

The preferred position change corresponds to the Euclidean or radial distance between the AS^{+} and AS^{-}conditions. The size ratio,σ_r, was calculated based on the following equation:

$$\sigma_r = \left(\frac{\sigma_{AS+} - \sigma_{AS-}}{\sigma_{AS-}} \right) \quad (3)$$

3.2. Connective field analysis

Repeated measures ANOVA, with ROI, condition (AS^{-}, AS^{+}SF), hemisphere and position bin as within-subject parameters, were used to compare the difference of the pRF preferred position and size between conditions. Participants were treated as random variables. For the AS^{+} condition, the pRF properties were estimated using two different models (FF, SF Fig. 2A). Separate statistical analyzes were performed for each of the resulting parameter sets. Permutation tests (1000 replications) were used to determine the significance level of the differences in CF size between conditions inside and outside the ASPZ. For this, data was aggregated over participants and condition labels were permuted.

All analyzes were performed using MATLAB (version 2018b; Mathworks, Natick, MA, USA) and R (version 2.11.1; R Foundation for Statistical Computing, Vienna, Austria). A p-value of 0.05 or less was considered significant.

4. Results

4.1. Perceptual filling-in of the AS

Fig. 3A shows the time required to fill in the scotomas for 6 of the 7 participants in the study. For all of them, filling-in occurred well within 60 secs, the time after which the retinotopic mapping stimuli were shown during the fMRI scanning. Fig. 3B shows the histogram of the gaze position during the trials in relation to the fixation point at the center of the screen. The probability density functions of both the horizontal and vertical components were centered at 0 deg. Moreover, their full width at half maximum (FWHF) was 0.65 deg and 1.19 deg for the horizontal and vertical components respectively. This indicates that the participants could maintain a stable fixation during the experiment.

To investigate if perceptual filling-in remained stable when during the retinotopic task, we compared the BOLD modulation of the voxels located at the ASPZ during AS+ and AS- conditions, if the moving bar disrupted the filling-in, we would expect to see an absence of a modulation of the time series in the AS^{+} condition, corresponding to an absence of activity (given that the AS was presented at mean background luminance). A voxel was considered to be contained within the ASPZ, if its pRF properties (center plus size) measured during the AS^{-}condition were confined to the AS location. Fig. 3C shows the average time series of the voxels within the four different AS projection zones for the con-

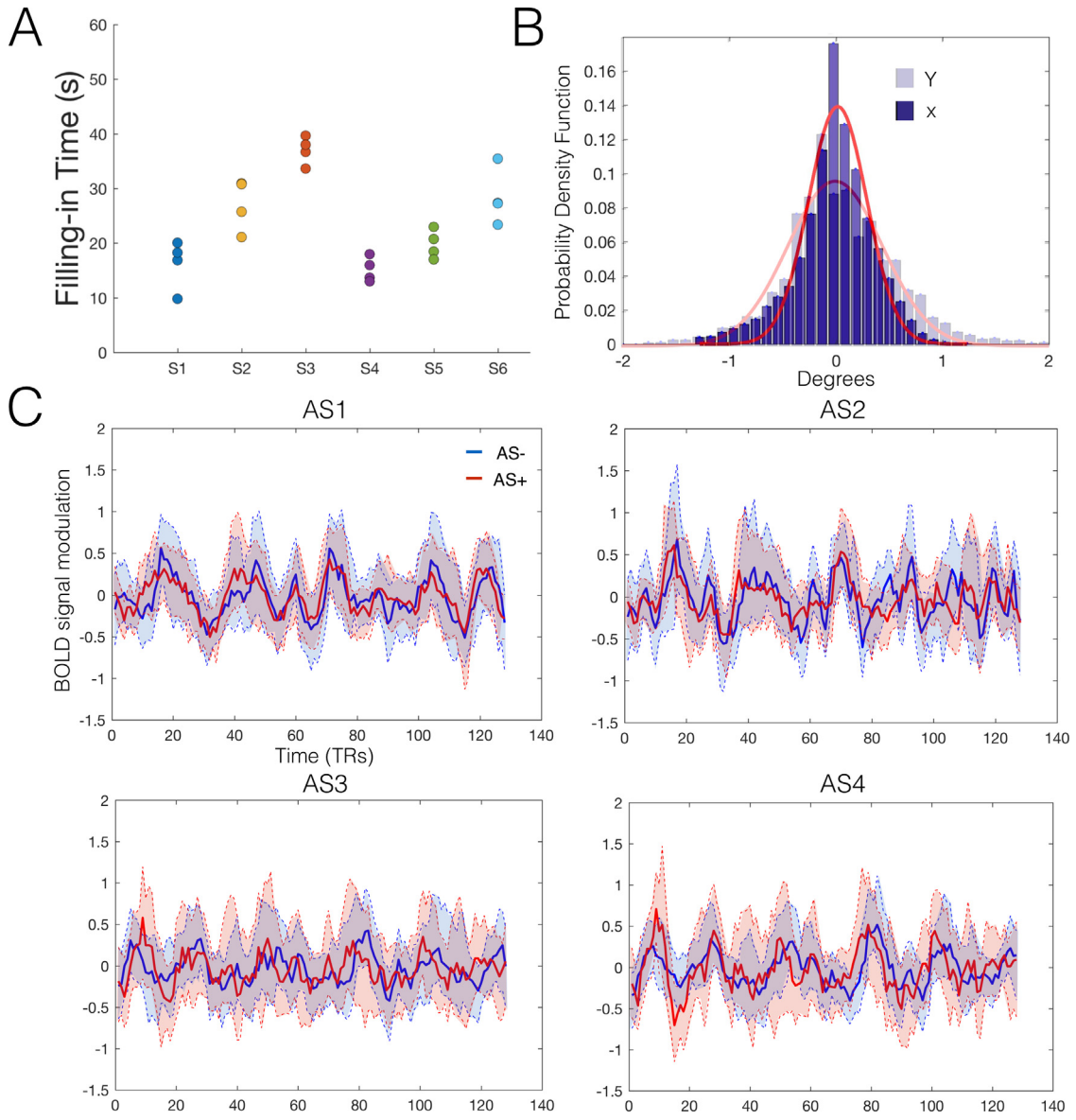

Fig. 3. Stable Filling-in effect during the AS+ condition. A: Results of the psychophysical tests used to define the adaptation time required in fMRI. Filling-in time as determined per trial and per participant. B: Histogram of the position of the eye (horizontal - x and vertical coordinates - y) relative to fixation. The fitted probability density function is depicted in red. C: For each AS, we show the average time series of the V1 voxels whose pRFs, as estimated for the AS- condition, fall entirely within the AS. The same voxels were used to derive the AS^{-} and AS^{+} condition-related time series. The dashed lines denote the 25 and 75% CI and are connected by shaded areas. Note: averaging the time series over the entire ASPZ most likely masked the local changes driven by the introduction of the AS. A total of 1913 V1 scotomatic voxels out of a total of 26,289 V1 voxels were included (around 137 voxels per V1 per hemisphere). (For interpretation of the references to color in this figure legend, the reader is referred to the web version of this article.).

ditions AS^{-} and AS^{+}. First, in the AS^{-} condition, we observe that the spatial frequency based contrast results in a decent fMRI response. Secondly, in the AS^{+} condition, even though the stimulation remains stable as there is no physical bar passing the scotoma, we observe very similar modulations (the cross correlations between the average AS^{-} and AS^{+} time series for AS1 are 0.74, 0.58, 0.54, 0.55, respectively). In the ASPZ of AS3 and AS4 there is even a higher modulation associated with the AS^{+} than with AS^{-} condition. In other words, despite the absence of a physical stimulus change, the modulation observed in the AS^{+} condition mimics the one observed during the AS^{-} condition. We interpret this as follows: similar to the actual bar, the filled-in bar is associated with a stronger response than the filled-in background. Thus, the filling-in induced response in the ASPZ is not constant, but modulates throughout the retinotopic mapping experiment. These findings support that throughout the AS^{+}condition, the AS were continuously masked, also when the bar moved over the AS. This agrees with the subjective experience of the participants that scotoma filling-in was stable throughout the experiment.

4.2. *The scotoma border attracts pRFs*

To examine the presence of changes in pRF properties between the AS^{-} and AS^{+} conditions obtained with the SF model, the data for the four different quadrants (each containing one AS) was collapsed onto a single quadrant. Next, the pRF properties of the voxels were spatially binned based on their preferred position as estimated in the AS^{-} condition. In visual area V1, following the presentation of an AS, pRFs with a preferred position originally inside the AS shifted radially outwards and towards the border of the AS (Fig. 4A). However, an analysis of the entire V1 representation showed that pRFs outside of the AS also appear to be

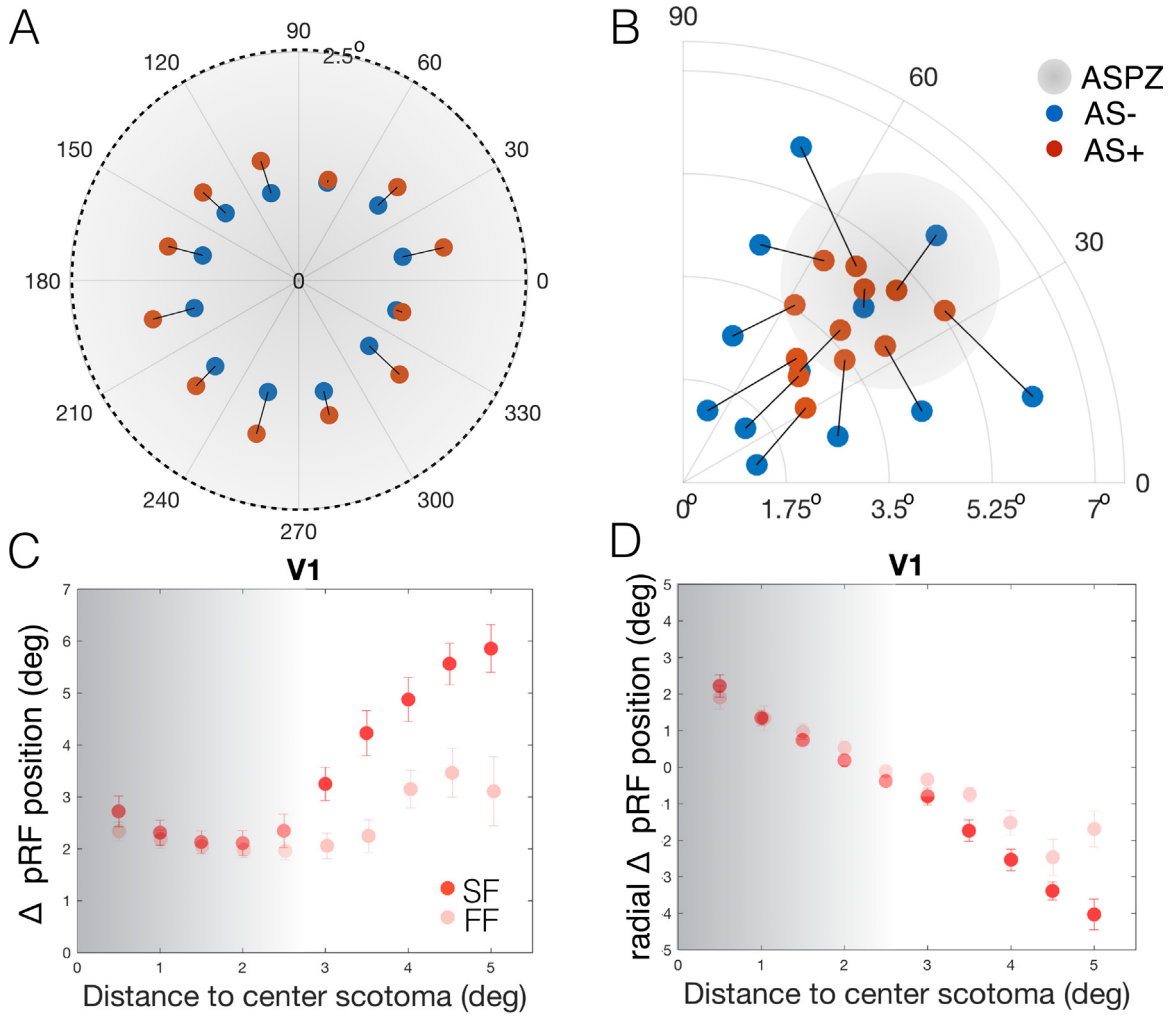

Fig. 4. V1 pRF position change in response to an AS. A: Shift between the two conditions AS$^-$ (blue) and AS$^+$ (red) of the pRFs with initial preferred positions located inside the ASPZ, averaged across participants. The dashed line represents the AS border and corresponds to 2.5 deg from the center of the AS. B: Average pRF location in various sectors of the visual field obtained for the AS$^-$ (blue) and AS$^+$ (red) conditions. The pRF properties shown in the panels A and B were calculated with the SF model. C: pRF position change (AS$^+$ vs AS$^-$) obtained with the SF and FF models as a function of distance between pRF position (based on AS$^-$) and the center of the scotoma (bins of 0.5 deg., Euclidean space). Error bars show the standard error of the mean over hemispheres. D: pRF position change obtained with the SF and FF models projected onto the radius as a function of the radial distance between pRF position measured in the AS$^-$ and the center of the scotoma. The gray transparent region refers to the AS, the darker region corresponds to the center of the AS. (For interpretation of the references to color in this figure legend, the reader is referred to the web version of this article.).

attracted towards the AS (Fig. 4B). These shifts were observed across the visual hierarchy (Figs. S2 and S3). We compared the preferred position in both conditions across the visual hierarchy using a two-way repeated measures ANOVA, which revealed main effects of condition (AS$^-$ versus AS$^+$, $F(1,6)=8.4$, $p = 0.004$) and ROI ($F(5,6) = 5.09$, $p = 0.003$). Furthermore the preferred position shifts were more pronounced for extrastriate areas (the interaction between ROI and condition was significant ($F(5,30)=7.87$, $p = 0.0034$)). Post hoc tests (FDR corrected) showed significant differences in position between conditions for all the visual areas tested ($p<0.001$). These observations suggest that pRFs throughout the visual field shifted their preferred position towards the AS border. When analyzed in more detail, Fig. 4C shows how the preferred position shifted obtained with the FF and SF models as a function of the pRFs' distance to the center of the AS. Note that in both models (SF and FF) the shift is minimal at the border (at 2.5 deg.). Fig. 4D plots the radial component of preferred position shift, again as a function of the pRFs distance to the AS center. For the SF model, this shows a nearly perfect linear relationship between the radial shift and the pRFs' initial preferred position ($r<-0.99$ and $p < 1 \times 10^{-8}$ for all the visual areas). Note that pRFs situated at the AS border hardly shift radially. Simulations of Euclidean and radial pRF position change resulting from arbitrary shifts in position (Fig. S4), excluded the possibility that these patterns are simply the result of statistical bias (regression to the mean, i.e. the probability that a pRF located in the fovea shifts to a more eccentric location is higher than that pRF shift to a more foveal location). In addition, we performed a test-retest analysis, to verify the stability of the observed shifts and to rule out that these are primarily the result of noise inherent to the binning in visual field sectors (Stoll et al., 2021). Figs. S5 and S6 confirm that the pRF estimates are reliable and the pRF shifts shown in Fig. 4 are at least four times larger than spurious shifts resulting from binning noisy pRF estimates.

To discard the possibility that the shifts in preferred pRF position are driven by model biases, i.e. partially stimulated pRFs near the border of the AS (Binda et al., 2013; Haak et al., 2012; Papanikolaou et al., 2015), we computed the RF profiles using an alternative approach, Microprobing (MP), which results in an pRF probe maps (Fig. 5B) rather than a 2D Gaussian parameters. Fig. 5 shows the pRF map obtained with MP for an ASPZ voxel during the conditions AS- and AS+ it is clear that the pRF gets displaced toward the edge of the AS (Fig. 5B). The modulation patterns of the time series are also clearly different, corroborating that

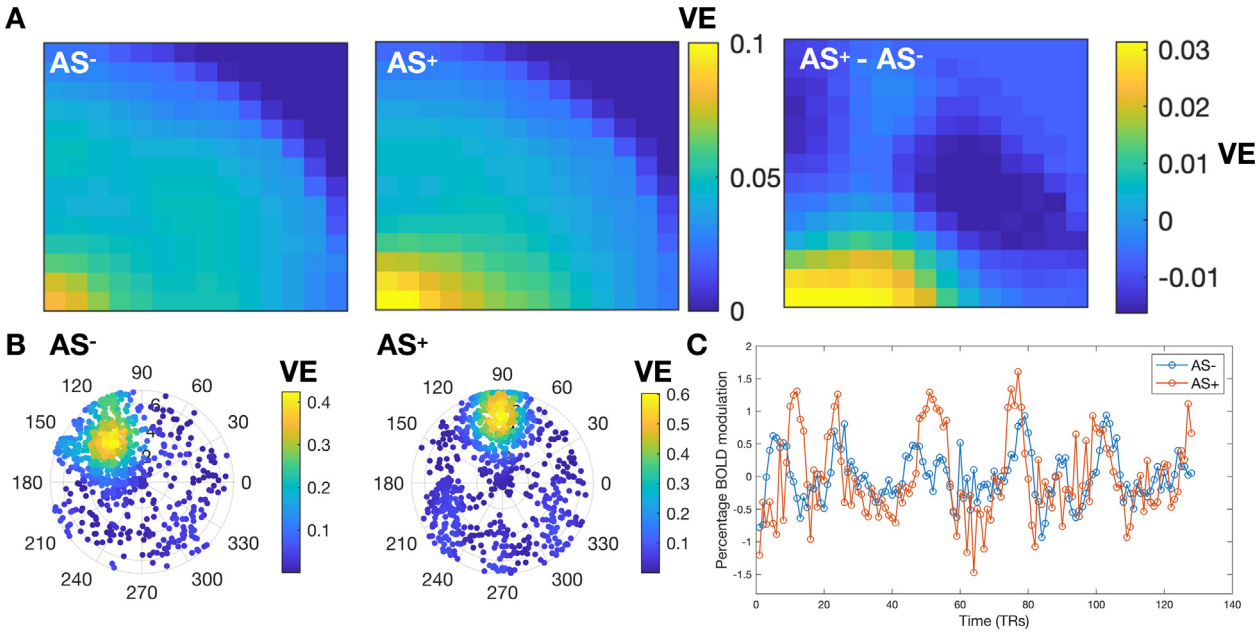

Fig. 5. V1 sampling density maps obtained with MP. A: Coverage maps for V1 in the AS^{-} and AS^{+} conditions and their difference (AS^{+}-AS^{-}). These maps were obtained by converting the probe maps into heat maps and aggregating these heat maps across all the voxels of V1. B: PRF probe maps obtained for a voxel located in the ASPZ for the AS^{-} and AS^{+} conditions. C: The BOLD modulation of the voxel shown in panel B in both the AS^{-} and AS^{+} conditions.

the shift in pRF preferred location cannot be just driven by a model bias (Fig. 5C). By aggregating the probe maps across a visual area we obtain a coverage map representing the sampling density of that area. Fig. 5A shows the VF coverage maps folded in quarter fields. The comparison between the AS- and AS+ VF coverage maps shows that during the AS+ there is a decrease in the sampling density of the AS and an increase in sampling in the VF regions surrounding the AS and of the central regions of the VF. These results are in agreement with what was found using the conventional pRF approach.

4.3. A gain field model explained the artificial scotoma induced pRF position shifts

The systematic changes in pRF preferred position suggest that these shifts may depend on their position relative to the AS border. Such shifts can be modeled using a gain field (GF) (Klein et al., 2014). To determine whether the border plays a critical role in the pRF reconfiguration, we first plotted the radial component of the shifts (Fig. 6A). This indicates that the shifts are of similar magnitude all around the perimeter of the AS (although different for pRFs initially inside or outside the AS). Next, we determined if we could predict the radial component in the AS^{+} condition based on the preferred positions in the AS^{-} condition by modulating the AS effect using a GF that is centered on the AS border, AS center and fixation (Fig. 6B). The GF model size was computed in two different ways: one is area-specific and another is common to all visual areas tested. Fig. 6 shows the predicted and measured pRF position shifts (Panel 6B) and size ratios (Panel 6C). The area-specific GF models centered at the border and center of the AS performed well as it explained (AS border: 59%, fixation: 9%, AS center:72%) of the variance in the radial position shifts and (border: 92%, fixation: 80%, AS center: 93%) of the size changes (Fig. 6B,C). The common GF model performed better than the area-specific GF model for the position prediction. It explained (AS border: 83%, fixation: 20%, AS center: 81%) of the variance in the radial position shifts and (AS border: 91%, fixation: 83%, AS center: 92%) of the size changes, respectively. The model centered at fixation could hardly explain the position shifts. The common GF centered at the border of the AS had a similar prediction accuracy as the common GF model centered on the AS. While the area specific GF model centered at the AS border performs better for V1, the gain model centered on the AS performs better for the remaining areas. The model comparison results can be found in Table 1. Nevertheless, we argue that the GF model centered at the border of the scotoma is most plausible because: 1) the visualization of the pRFs in- and outside of the ASPZ shows that all tend to shift towards the border, 2) at the level of V1, the GF model at the border has more explanatory power than the one centered on the AS, 3) the common GF model centered at the AS border performs better for V1,V2, LO1 and LO2 than the on centered on the AS, and 4) due to the pooling of information throughout the visual hierarchy, pRF shifts measured in areas beyond V1 are most likely affected by the V1 shifts.

Fig. 6D shows that the position predictions of the AS border GF model are more accurate for the higher compared to the lower order areas, (using the AS border model V1, variance explained of 44% (area specific GF) and 62% (common GF); LO1, variance explained of 73% (area specific GF) and 97% (common GF)). The preferred position shifts tend to increase along the visual hierarchy. Although the pRF sizes increased with eccentricity and visual hierarchy (Pearson's correlation coefficient: $r^2 > 0.8$ and $p < 0.05$ for all visual areas tested), the pRF preferred position change does not correlate strongly with the pRF size within each visual field map (V1 $r = 0.06$; V2 $r = -0.06$; V3 $r = 0.13$; V4 $r = -0.06$; LO1 $r = 0.1$; LO2 $r = -0.2$; all $p < 0.0005$).

Regarding the changes in pRF size, a comparison across condition and visual areas revealed that it does not change significantly between conditions ($F(1,6)=0.007$, $p = 0.93$) but it does change with visual area ($F(5,6)=6.5$, $p < 0.0001$), while the interaction between condition and visual area is not significant ($F(5,30)=0.63$, $p = 0.67$). Post hoc tests (FDR corrected) did not show any significant differences in pRF size between any of the conditions tested (AS^{-}, AS^{+}SF, AS^{+}FF; $p>0.09$).

4.4. Neural populations in extrastriate cortex increase their V1 sampling region

Visual areas beyond V1 may also respond to the AS by changing their V1 sampling. Changes in sampling of a source area such as V1 can be quantified by modeling the connective field (CF) of the recording site. A CF predicts the neuronal activity of a recording site (voxel) in a target region (e.g. V2) given the activity in another part of the brain (e.g.

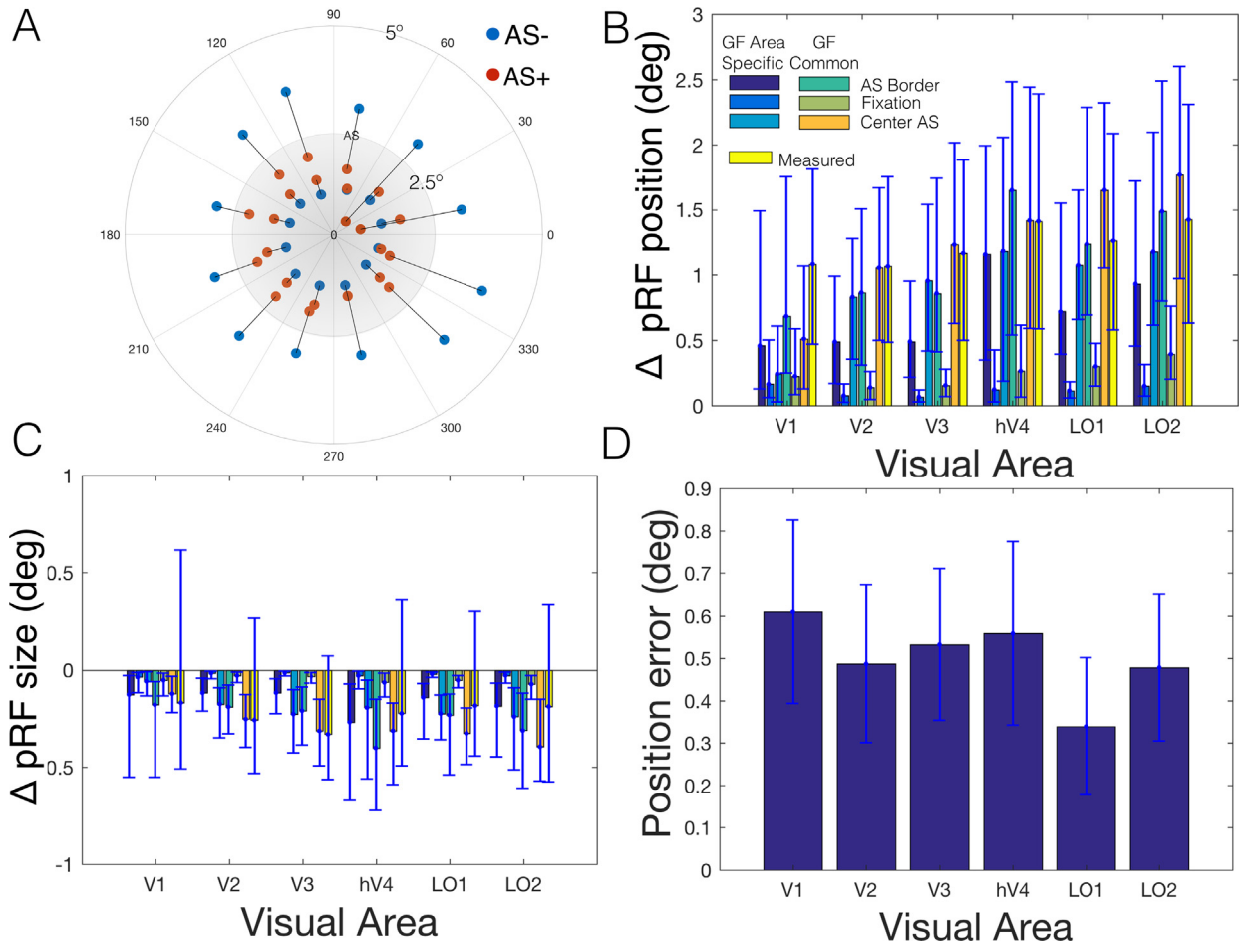

Fig. 6. A gain field model centered at the AS border explains changes in preferred population RF position. A: Radial position change between the two conditions AS^{-} (blue) and AS^{+} (red) in various sectors of the visual field inside and outside the AS, averaged across participants. The gray region corresponds to the ASPZ. The eccentricity lines correspond to 2.5° and 5°. B/C: Measured (yellow) and predicted, using an area-specific (blue) and common (green and orange) GF centered at the border of the AS, center of the AS andat fixation, RF position shifts (B) and size changes (C) in response to an AS. D: Mean average error between the predicted using a gain field centered at the border of the scotoma and measured pRF shifts. The error bars represent the 95% confidence interval across the voxels in the test set. The estimated GF size did not vary significantly between visual areas ($F = 0.16$; $p = 0.97$). All the panels depict the aggregate results for the pRFs located both inside and outside of the artificial scotoma projection zone. (For interpretation of the references to color in this figure legend, the reader is referred to the web version of this article.).

Table 1
GF Model comparison based on BIC. BIC between the predicted position and size of the estimated pRFs using the different GF models (Border, Fixation and Center) and measured pRF estimates, for the different visual areas. The most explanatory model (the one with the lowest BIC) is highlighted.

Bayesian Information Criteria (BIC)												
Visual Areas	Position						Size					
	Area specific GF			Common GF			Area specific GF			Common GF		
	Border	Fixation	Center	Border	Fixation	Center	Border	Fixation	Center	Border	Fixation	Center
V1	**11,565**	11,625	11,584	**11,533**	11,609	11,592	24,888	24,896	**24,873**	24,855	24,874	**24,815**
V2	13,321	13,881	**13,288**	**13,362**	13,848	13,373	28,735	28,732	**28,652**	28,640	28,703	**28,595**
V3	13,050	14,125	**12,733**	12,948	14,086	**12,825**	24,754	24,766	**24,703**	24,690	24,749	**24,657**
hV4	6357	6557	**6115**	6269	6551	**6107**	**9968**	10,135	10,101	**9859**	10,075	9971
LO1	12,325	12,851	**12,028**	**11,974**	12,841	12,039	20,179	20,241	**20,087**	29,140	20,214	**20,049**
LO2	9738	10,031	**9697**	**9748**	10,028	9784	15,576	15,627	**15,493**	15,525	15,602	**15,445**

V1). Assessing CF properties is useful for various reasons: 1) it informs how information is integrated along the visual hierarchy; 2) it has the potential to capture the neural circuits underlying pRF dynamics, such as feedback signals; 3) CFs are stimuli agnostic and are estimated without modeling the stimulus, so they are not subject to modeling bias, and 4) CFs are shaped by internal connectivity, so they isolates changes in connectivity from those in the pRFs of the source area. Fig. 7A shows the difference in CF size between the two AS conditions (AS^{+} - AS^{-}) for the voxels whose preferred position was initially located either inside or outside the ASPZ. The CF of the voxels initially inside the ASPZ became larger following the introduction of the AS (Panels A and B). Fig. 7B shows the cumulative histogram of the CF sampling extent for ASPZ of the visual areas tested. Note that the V1 sampling extent increases with visual hierarchy. This trend is not present for the voxels located out-

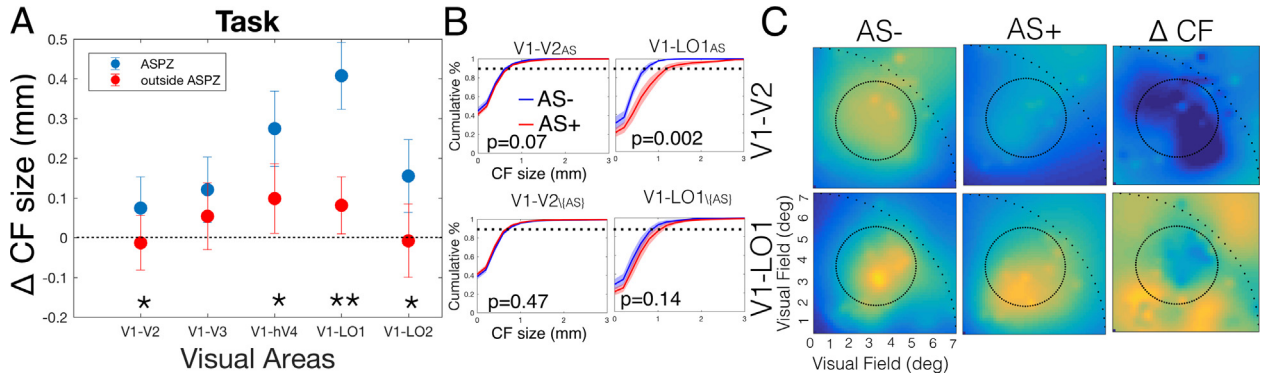

Fig. 7. Changes in cortico-cortical connections in response to AS. A: Difference in the cumulative distribution at the 90% point of the difference in CF size (AS^+ - AS^-) for voxels situated inside (blue) and outside (red) of the ASPZ. The error bars represent the 95% CI. This delta CF size differed significantly for voxels inside and outside the ASPZ for areas V2, hV4, LO1 and LO2 ($p < 0.001$), represented in the graph by a *. The levels of significance were calculated using permutation statistics, explained in detail in the methods under statistical analysis. B: Top graphs: Cumulative percentage of the CF size for the conditions AS^- (blue) and AS^+ (red) calculated for the voxels within the ASPZ in the target visual areas V2 and LO1. Bottom graphs: Analogous analysis to the top graphs, but for those voxels outside the ASPZ. The shaded area represents the 95% confidence interval. The p-value on the bottom right of each graph shows the significance of the difference between the two conditions. C: Coverage map of CFs obtained for AS^-, AS^+ and the delta CF size. To isolate CF changes from any pRF changes, for both conditions, the back projection onto the visual field was performed based on the pRF estimates obtained with AS^-. The sparse dotted line depicts the visual stimulation area and the dense dotted line the AS location in the visual field. Each map represents the combined data from 7 subjects. (For interpretation of the references to color in this figure legend, the reader is referred to the web version of this article.).

side the ASPZ. In particular, LO1 inside the ASPZ sampled from a larger region of V1, which is evident from the increased CF size. This effect was not clearly present for locations outside the ASPZ (bottom graph on Panel B; LO1: inside ASPZ, $p = 0.002$; outside ASPZ $p = 0.140$). To show how the accumulation of these changes influence the sampling of V1, we projected the CFs back into visual field space by convolving them with the V1 pRFs from which they sample. To isolate AS-induced changes in the CFs from those in the pRFs of V1, the CFs of both the AS^- and AS^+ conditions were back projected using the same set of pRFs (those from the AS^- condition). For areas V2 and LO1, Fig. 7C shows the CF sampling density in the conditions AS^- and AS^+ and their difference (AS^+ - AS^-). For the ASPZ, V2 sampling density is reduced in the AS^+ compared to the AS^-condition. The ΔCF image shows that the introduction of the AS generally resulted in a reduction of the sampling of V1 AS region and a denser sampling of V1 regions outside the ASPZ. This effect is particularly pronounced in LO1. To confirm that we isolated changes in connectivity from changes in the pRFs, we regressed out the stimulus driven responses. Fig. S10 shows that variation is CF size and the CF coverage maps obtained with the original signal are similar to those obtained with the task regressed out signal.

5. Discussion

Our main finding is that the introduction of an artificial scotoma (AS) into the visual field results in an extensive, system-wide reconfiguration of neural population properties. Throughout the visual hierarchy, the pRFs located in- and outside of the ASPZ shift their prefered position towards the AS border. Simultaneously, extrastriate areas bias their processing towards signals coming from sections of V1 not covered by the AS, thereby effectively masking it. Gain field models, centered either at the border or the center of the AS, best explain the pRF shifts in extrastriate regions. Therefore, we suggest that the signals driving these modifications originate in extrastriate areas and, through feedback, reconfigure the neural populations in earlier visual areas.

5.1. An artificial scotoma induces a visual system-wide reconfiguration of population receptive fields

Shifts in preferred position have previously been reported for the pRFs initially located inside the PZ of both natural scotoma and AS (Baseler et al., 2011; Binda et al., 2013; Haak et al., 2012; Papanikolaou et al., 2015; Barton and Brewer, 2015). Our study is the first to show that such a reconfiguration is a visual system-wide phenomenon. Within the ASPZ, pRFs shifted their preferred position towards the AS border. We find that pRFs initially located outside the ASPZ shifted their preferred position towards the AS border as well. Our observed preferred position shifts were not accompanied by simultaneous increases in pRF size, as previously reported for both retinal and cortical scotomas (Gilbert and Wiesel, 1992; Pettet and Gilbert, 1992).

5.2. Origin of pRF shifts

Previous studies have suggested that changes in pRFs in response to an AS can result from a model bias driven by partial stimulation of the neuronal populations (Binda et al., 2013; Haak et al., 2012; Papanikolaou et al., 2015). Such bias can be avoided by accounting for the presence of the AS during the pRF modeling (Binda et al., 2013; Papanikolaou et al., 2015). We modeled the pRFs assuming either the presence of the AS (SF model) or not (FF model). We found similar positional shifts within the ASPZ with either approach, indicating that our findings are likely not due to model bias. In principle, pRF model bias could also be reduced by using multifocal retinotopic stimulation. However, we could not use this since the rapid stimulus changes during multifocal stimulation would have entirely disrupted PM. We verified that the estimated pRFs are reliable, and that the effect of noise and binning approach cannot explain the pRF shifts measured (Figs. S5, S6 and S9). Moreover, we find that the presence of a dynamic noise background during retinotopic mapping has little effect on the estimated pRF positions (Fig. S8). Moreover, changes in estimated pRFs properties are caused by differently shaped BOLD signals, not different signal amplitudes (Carvalho et al., 2019). This implies that the changes in preferred pRF positions are genuine and not simply due to the reduced stimulus contrast in the AS.

5.3. Illusory predictive signals

The predictability of the moving bar might have generated anticipatory signals at its future location (Binda et al., 2013; Kastner et al., 1999), which are difficult to distinguish from PM related signals. However, this notion does not affect the interpretation of our results. First, any movement anticipation would have similarly influenced the AS^- and AS^+ conditions. Second, during the AS^+ condition the participants

reported to have filled-in the bar. This cannot be explained by predictability alone. Third, previously, it has been shown that an AS can be mapped by back-projecting into the visual field the pRFs estimated in an experiment that used a predictable moving bar (Carvalho et al., 2021; Hummer et al., 2018; Ritter et al., 2019). This is only possible in the absence of pRFs that sample the scotomatic visual field. Fourth, the pRF shifts expected on the basis of bar anticipation (Binda et al., 2013; Kastner et al., 1999) are inconsistent with the pRF shifts that we observed. Specifically, we find no evidence for pRF size changes either inside or outside the ASPZ. Moreover, the pRFs not spanning the AS are also attracted towards the scotoma border. We cannot exclude that a small part of the pRF position shifts observed in this study may be driven by measurement noise, and may thus also be observed in the absence of filling-in. However, in general such shifts would be much smaller and lack the directional specificity that we observed for the shifts induced by the AS.

5.4. Attention

Although the participants were filling-in the AS during the experiment the borders of the AS become salient, which will draw attention to that region. Attentional suppression at the level of early visual areas may reduce the neural activity in the regions surrounding the scotoma. Importantly the gain field explores how attention can modulate the pRFs.

5.5. A gain field at the scotoma border explains the shifts in pRF preferred position

As indicated, the pRF shifts were predominantly directed towards the AS border. A biologically motivated GF that accounts for the presence of the AS explains these shifts. This suggests that the presence of an AS results in a reweighting of the spatial response selectivity towards the scotomatic border. For V1, a gain field model centered at the AS border outperformed a model centered on the AS. For other areas, both types of model performed equally well. This may be explained by the increase in average pRF size along the cortical hierarchy - larger pRFs will be simultaneously attracted by multiple sites on the AS border, mimicking an attraction by the AS center. The resulting reweighting may result from a combination of feedforward and feedback signals (Klein et al., 2018). Gain fields have previously been used to model attention induced shifts in pRFs as well (Klein et al., 2014; Womelsdorf et al., 2006). Therefore, gain fields may be an important mechanism by which the brain can flexibly adapt its computational resources to the task at hand.

5.6. Extrastriate cortex biases its sampling of V1 towards outside of the ASPZ

By quantifying the CFs of extrastriate target areas (V2 to LO2), we described how these areas sample source area V1. We performed this analysis both on the original time-series, and on the time-series which had the task-related signal regressed out (Fig. S10). In both cases, the introduction of AS, results in larger CF within the ASPZ, whereas CF outside of it do not change. For V2-LO2, this increases their sampling of V1 outside of the ASPZ and reduces their sampling of the V1 ASPZ region. This effect was most prominent for LO1. Thus, following the presentation of an AS, cortico-cortical connections reconfigure such that more information is captured from outside than inside the ASPZ. This is consistent with PM and suggests that changes in intra-area connectivity underlie PM.

5.7. Feedback from extrastriate regions may drive the visual system-wide reconfiguration

In our analysis, the gain field model centered on the AS border best explained the observed pRF modulations in extrastriate area LO1. LO1 plays a major role in the processing of oriented boundaries or borders (Larsson and Heeger, 2006; Silson et al., 2013) and its role can be dissociated from that of LO2, which preferably processes shape (Silson et al., 2013). Moreover, also the CF changes that resulted in increased sampling of V1 was most prominent for LO1. Therefore, we propose that extrastriate feedback signals that, most likely, originate in LO1 underlie the reconfiguration of neural populations in response to an AS. This notion is consistent with other studies showing that the responsiveness of early visual cortical areas can be modulated by feedback from extrastriate cortex (Morgan et al., 2018; Muckli et al., 2015; Kok et al., 2016).

While the influence of an AS is acute, natural scotomas take a long time to develop. In such cases, structural changes may develop in response to prolonged acute functional changes that we observe with AS. Natural scotomas are present for a long period of time (years) and thus would facilitate long-term adaptive processes as it is metabolically costly to maintain a sustained state via fast responding processes (Haak and Beckmann, 2019). Nevertheless, we consider AS an useful model of natural scotomas, as it allows us to predict what type of neural and perceptual changes these may evoke. Indeed, previous studies found similar functional changes in pRF properties and connectivity to occur for patients with natural scotomas and control observers with AS (Baseler et al., 2011; Haak et al., 2012). The acute changes in pRFs and CFs are consistent with PM being a short-term plasticity process. Its neural bases could be changes in neural gain that alter the balance between input and feedback signals and modify the spatial response modulations of neurons in the primary visual cortex (Baseler et al., 2011; Haak et al., 2012).

5.8. Limitations and future studies

Although binning is a standard approach in data analyzes, in case of noisy data, such as BOLD signals, grouping pRFs across multiple conditions according to bins defined on the basis of the data of a single condition may lead to biases in the results. Such biases may resemble shifts in pRF position (Stoll et al., 2021). In our study, a test-retest analysis indicates that the magnitude of noise induced spurious shifts accounted for at most a quarter of the observed pRF shifts measured. Nevertheless, in our view, future studies should avoid a possible influence of binning-induced bias by including independent runs to be used exclusively for the binning, sufficient data to allow for test-retest analysis, and obtain replication data.

In our experiment, eye movements were not recorded during scanning but were minimized by having observers perform an attention demanding task at fixation. Remaining eye movements may bias pRF estimates and would have resulted in increased pRF sizes (Hummer et al., 2016; Klein et al., 2014; Levin et al., 2010), which we did not find.

Measuring the neuronal mechanisms associated with PM at a finer scale could reveal subtle changes that remain hidden at a coarser scale. For example, more pRFs can be identified in the ASPZ, and laminar profiles across cortical depth could be determined. The latter would be essential to find the origins of the feedback and feedforward signals contributing to PM and modulating perception.

Data and code availability statement

The data that support the findings of this study is openly available at XNAT central under the project ID: fMRI_PM

The code for the gain field model and connective field backprojections is available in the following links: https://github.com/Joana-Carvalho/Gain-field-model https://github.com/Joana-Carvalho/Connective-field-back-projection

CRediT authorship contribution statement

Joana Carvalho: Conceptualization, Data curation, Methodology, Formal analysis, Writing – original draft. **Remco J. Renken:** Method-

ology, Writing – review & editing, Supervision. **Frans W. Cornelissen:** Conceptualization, Methodology, Writing – review & editing, Supervision, Funding acquisition.

Declaration of Competing Interest

None.

Credit authorship contribution statement

Joana Carvalho: Conceptualization, Data curation, Methodology, Formal analysis, Writing – original draft. **Remco J. Renken:** Methodology, Writing – review & editing, Supervision. **Frans W. Cornelissen:** Conceptualization, Methodology, Writing – review & editing, Supervision, Funding acquisition.

Acknowledgments

Author JC was supported by the European Union's Horizon 2020 research and innovation program under the Marie Sklodowska-Curie grant agreement No. 641805 (NextGenVis) and No 101032056 (PlastiMap), and by a grant from the Graduate School of Medical Sciences of the University Medical Center Groningen. The funding organizations had no role in the design, conduct, analysis, or publication of this research.

Supplementary materials

Supplementary material associated with this article can be found, in the online version, at doi:10.1016/j.neuroimage.2021.118690.

References

Angelucci, A., Levitt, J.B., Lund, J.S., 2002. Anatomical origins of the classical receptive field and modulatory surround field of single neurons in macaque visual cortical area V1. Prog. Brain Res. 136, 373–388.
Baker, C.I., Peli, E., Knouf, N., Kanwisher, N.G., 2005. Reorganization of visual processing in macular degeneration. J. Neurosci. 25, 614–618.
Barton, B., Brewer, A.A., 2015. fMRI of the rod scotoma elucidates cortical rod pathways and implications for lesion measurements. Proc. Natl. Acad. Sci. U. S. A. 112, 5201–5206.
Baseler, H.A., Gouws, A., Haak, K.V., Racey, C., Crossland, M.D., Tufail, A., Rubin, G.S., Cornelissen, F.W., Morland, A.B., 2011. Large-scale remapping of visual cortex is absent in adult humans with macular degeneration. Nat. Neurosci. 14, 649–655.
Binda, P., Thomas, J.M., Boynton, G.M., Fine, I., 2013. Minimizing biases in estimating the reorganization of human visual areas with BOLD retinotopic mapping. J. Vis. 13, 13.
Brainard, D.H., 1997. The psychophysics toolbox. Spat. Vis. 10, 433–436.
Calford, M.B., 2002a. Dynamic representational plasticity in sensory cortex. Neuroscience 111, 709–738.
Calford, M.B., 2002b. Mechanisms for acute changes in sensory maps. Adv. Exp. Med. Biol. 508, 451–460.
Carvalho, J., Invernizzi, A., Ahmadi, K., Hoffmann, M.B., Renken, R.J., Cornelissen, F.W., 2020. Micro-probing enables fine-grained mapping of neuronal populations using fMRI. Neuroimage 209, 116423.
Carvalho, J., Invernizzi, A., Martins, J., Jansonius, N.M., Renken, R.J., Cornelissen, F.W., 2021. Visual field reconstruction using fMRI-based techniques. Transl. Vis. Sci. Technol. 13, 10–25.
Carvalho, J., Renken, R.J., Cornelissen, F.W., 2019. Studying cortical plasticity in ophthalmic and neurological disorders: from stimulus-driven to cortical circuitry modeling approaches. Neural Plast. 2019, 2724101.
Chen, Y., Anand, S., Martinez-Conde, S., Macknik, S.L., Bereshpolova, Y., Swadlow, H.A., Alonso, J.M., 2009. The linearity and selectivity of neuronal responses in awake visual cortex. J. Vis. 9, 12.1–1217.
Clifford, C.W.G., Webster, M.A., Stanley, G.B., Stocker, A.A., Kohn, A., Sharpee, T.O., Schwartz, O., 2007. Visual adaptation: neural, psychological and computational aspects. Vis. Res. 47, 3125–3131.
Cornelissen, F.W., Peters, E.M., Palmer, J., 2002. The eyelink toolbox: eye tracking with MATLAB and the psychophysics toolbox. Behav. Res. Methods Instrum. Comput. doi:10.3758/bf03195489.
Dale, A.M., Fischl, B., Sereno, M.I., 1999. Cortical surface-based analysis. I. Segmentation and surface reconstruction. Neuroimage 9, 179–194.
Das, A., Gilbert, C.D., 1995. Long-range horizontal connections and their role in cortical reorganization revealed by optical recording of cat primary visual cortex. Nature doi:10.1038/375780a0.
DeAngelis, G.C., Anzai, A., Ohzawa, I., Freeman, R.D., 1995. Receptive field structure in the visual cortex: does selective stimulation induce plasticity? Proc. Natl. Acad. Sci. U. S. A. 92, 9682–9686.
De Weerd, P., Gattass, R., Desimone, R., Ungerleider, L.G., 1995. Responses of cells in monkey visual cortex during perceptual filling-in of an artificial scotoma. Nature 377, 731–734.
De Weerd, P., Smith, E., Greenberg, P., 2006. Effects of selective attention on perceptual filling-in. J. Cogn. Neurosci. 18, 335–347.
Dilks, D.D., Baker, C.I., Liu, Y., Kanwisher, N., 2009. Referred visual sensations": rapid perceptual elongation after visual cortical deprivation. J. Neurosci. 29, 8960–8964.
Dilks, D.D., Serences, J.T., Rosenau, B.J., Yantis, S., McCloskey, M., 2007. Human adult cortical reorganization and consequent visual distortion. J. Neurosci. 27, 9585–9594.
Dreher, B., Burke, W., Calford, M.B., 2001. Chapter 15 Cortical plasticity revealed by circumscribed retinal lesions or artificial scotomas. Prog. Brain Res. doi:10.1016/s0079-6123(01)34016-5.
Dumoulin, S.O., Wandell, B.A., 2008. Population receptive field estimates in human visual cortex. Neuroimage 39, 647–660.
Enroth-Cugell, C., Freeman, A.W., 1987. The receptive-field spatial structure of cat retinal Y cells. J. Physiol. doi:10.1113/jphysiol.1987.sp016443, (Lond.).
Fiorani Júnior, M., Rosa, M.G., Gattass, R., Rocha-Miranda, C.E., 1992. Dynamic surrounds of receptive fields in primate striate cortex: a physiological basis for perceptual completion? Proc. Natl. Acad. Sci. U. S. A. 89, 8547–8551.
Gilbert, C.D., Wiesel, T.N., 1992. Receptive field dynamics in adult primary visual cortex. Nature doi:10.1038/356150a0.
Gravel, N., Harvey, B., Nordhjem, B., Haak, K.V., Dumoulin, S.O., Renken, R., Curčić-Blake, B., Cornelissen, F.W., 2014. Cortical connective field estimates from resting state fMRI activity. Front. Neurosci. 8, 339.
Haak, K.V., Beckmann, C.F., 2019. Plasticity versus stability across the human cortical visual connectome. Nat. Commun. 10, 3174.
Haak, K.V., Cornelissen, F.W., Morland, A.B., 2012. Population receptive field dynamics in human visual cortex. PLoS One 7, e37686.
Haak, K.V., Morland, A.B., Engel, S.A., 2015. Plasticity, and its limits, in adult human primary visual cortex. Multisens. Res. 28, 297–307.
Haak, K.V., Winawer, J., Harvey, B.M., Renken, R., Dumoulin, S.O., Wandell, B.A., Cornelissen, F.W., 2013. Connective field modeling. Neuroimage 66, 376–384.
Harrison, W.J., Ayeni, A.J., Bex, P.J., 2019. Attentional selection and illusory surface appearance. Sci. Rep. 9, 2227.
Hoste, A.M., 2003. New insights into the subjective perception of visual field defects. Bull. Soc. Belge Ophtalmol. 287, 65–71.
Hummer, A., Ritter, M., Tik, M., Ledolter, A.A., Woletz, M., Holder, G.E., Dumoulin, S.O., Schmidt-Erfurth, U., Windischberger, C., 2016. Eyetracker-based gaze correction for robust mapping of population receptive fields. Neuroimage 142, 211–224.
Hummer, A., Ritter, M., Woletz, M., Ledolter, A.A., Tik, M., Dumoulin, S.O., Holder, G.E., Schmidt-Erfurth, U., Windischberger, C., 2018. Artificial scotoma estimation based on population receptive field mapping. Neuroimage 169, 342–351.
Kapadia, M.K., Gilbert, C.D., Westheimer, G., 1994. A quantitative measure for short-term cortical plasticity in human vision. J. Neurosci. 14, 451–457.
Kastner, S., Pinsk, M.A., De Weerd, P., Desimone, R., Ungerleider, L.G., 1999. Increased activity in human visual cortex during directed attention in the absence of visual stimulation. Neuron 22, 751–761.
Klein, B.P., Fracasso, A., van Dijk, J.A., Paffen, C.L.E., Te Pas, S.F., Dumoulin, S.O., 2018. Cortical depth dependent population receptive field attraction by spatial attention in human V1. Neuroimage 176, 301–312.
Klein, B.P., Harvey, B.M., Dumoulin, S.O., 2014. Attraction of position preference by spatial attention throughout human visual cortex. Neuron 84, 227–237.
Kohn, A., 2007. Visual adaptation: physiology, mechanisms, and functional benefits. J. Neurophysiol. 97, 3155–3164.
Kok, P., Bains, L.J., van Mourik, T., Norris, D.G., de Lange, F.P., 2016. Selective activation of the deep layers of the human primary visual cortex by top-down feedback. Curr. Biol. 26, 371–376.
Komatsu, H., 2006. The neural mechanisms of perceptual filling-in. Nat. Rev. Neurosci. 7, 220–231.
Larsson, J., Heeger, D.J., 2006. Two retinotopic visual areas in human lateral occipital cortex. J. Neurosci. 26, 13128–13142.
Levin, N., Dumoulin, S.O., Winawer, J., Dougherty, R.F., Wandell, B.A., 2010. Cortical maps and white matter tracts following long period of visual deprivation and retinal image restoration. Neuron 65, 21–31.
Masuda, Y., Dumoulin, S.O., Nakadomari, S., Wandell, B.A., 2008. V1 projection zone signals in human macular degeneration depend on task, not stimulus. Cereb. Cortex 18, 2483–2493.
Mendola, J.D., Conner, I.P., Sharma, S., Bahekar, A., Lemieux, S., 2006. fMRI measures of perceptual filling-in in the human visual cortex. J. Cogn. Neurosci. 18, 363–375.
Morgan, A., Petro, L., Muckli, L., 2018. Cortical feedback to superficial layers of V1 contains predictive scene information. In: Proceedings of the Conference on Cognitive Computational Neuroscience doi:10.32470/ccn.2018.1083-0.
Muckli, L., De Martino, F., Vizioli, L., Petro, L.S., Smith, F.W., Ugurbil, K., Goebel, R., Yacoub, E., 2015. Contextual feedback to superficial layers of V1. Curr. Biol. 25, 2690–2695.
Nestares, O., Heeger, D.J., 2000. Robust multiresolution alignment of MRI brain volumes. Magn. Reson. Med. 43, 705–715.
Papanikolaou, A., Keliris, G.A., Lee, S., Logothetis, N.K., Smirnakis, S.M., 2015. Nonlinear population receptive field changes in human area V5/MT+ of healthy subjects with simulated visual field scotomas. Neuroimage 120, 176–190.
Parks, N.A., Corballis, P.M., 2012. Neural mechanisms of short-term plasticity in the human visual system. Cereb. Cortex doi:10.1093/cercor/bhr368.
Pelli, D.G., 1997. The videotoolbox software for visual psychophysics: transforming numbers into movies. Spat. Vis. 10, 437–442.
Pessoa, L., De Weerd, P., 2003. Filling-In: From Perceptual Completion to Cortical Reorganization. Oxford University Press.

Pettet, M.W., Gilbert, C.D., 1992. Dynamic changes in receptive-field size in cat primary visual cortex. Proc. Natl. Acad. Sci. U. S. A. 89, 8366–8370.
Ramachandran, V.S., Gregory, R.L., Aiken, W., 1993. Perceptual fading of visual texture borders. Vis. Res. 33, 717–721.
Rao, R.P., Ballard, D.H., 1999. Predictive coding in the visual cortex: a functional interpretation of some extra-classical receptive-field effects. Nat. Neurosci. 2, 79–87.
Reynolds, J.H., Heeger, D.J., 2009. The normalization model of attention. Neuron 61, 168–185.
Ritter, M., Hummer, A., Ledolter, A.A., Holder, G.E., Windischberger, C., Schmidt-Erfurth, U.M., 2019. Correspondence between retinotopic cortical mapping and conventional functional and morphological assessment of retinal disease. Br. J. Ophthalmol. 103, 208–215.
Silson, E.H., McKeefry, D.J., Rodgers, J., Gouws, A.D., Hymers, M., Morland, A.B., 2013. Specialized and independent processing of orientation and shape in visual field maps LO1 and LO2. Nat. Neurosci. 16, 267–269.
Smirnakis, S.M., Brewer, A.A., Schmid, M.C., Tolias, A.S., Schüz, A., Augath, M., Inhoffen, W., Wandell, B.A., Logothetis, N.K., 2005. Lack of long-term cortical reorganization after macaque retinal lesions. Nature 435, 300–307.
Smith, N.D., Crabb, D.P., Glen, F.C., Burton, R., Garway-Heath, D.F., 2012. Eye movements in patients with glaucoma when viewing images of everyday scenes. Seeing Perceiving 25, 471–492.
Spillmann, L., Kurtenbach, A., 1992. Dynamic noise backgrounds facilitate target fading. Vis. Res. 32, 1941–1946.
Spratling, M.W., 2010. Predictive coding as a model of response properties in cortical area V1. J. Neurosci. 30, 3531–3543.
Stoll, S., Infanti, E., Haas, B., Schwarzkopf, S.D., 2021. Flaws in Data Binning For Population Receptive Field Analyzes. Biorxiv doi:10.1101/2020.12.15.422942.
Tailby, C., Metha, A., 2004. Artificial scotoma-induced perceptual distortions are orientation dependent and short lived. Vis. Neurosci. 21, 79–87.
Tremere, L.A., Pinaud, R., De Weerd, P., 2003. Contributions of inhibitory mechanisms to perceptual completion and cortical reorganization. Filling-In: From Perceptual Completion to Cortical Reorganization (Pessoa). Oxford University Press, pp. 295–322.
Wandell, B.A., Chial, S., Backus, B.T., 2000. Visualization and measurement of the cortical surface. J. Cogn. Neurosci. 12, 739–752.
Wandell, B.A., Smirnakis, S.M., 2009. Plasticity and stability of visual field maps in adult primary visual cortex. Nat. Rev. Neurosci. 10, 873–884.
Weil, R.S., Rees, G., 2011. A new taxonomy for perceptual filling-in. Brain Res. Rev. 67, 40–55.
Weil, R.S., Watkins, S., Rees, G., 2008. Neural correlates of perceptual completion of an artificial scotoma in human visual cortex measured using functional MRI. Neuroimage 42, 1519–1528.
Womelsdorf, T., Anton-Erxleben, K., Pieper, F., Treue, S., 2006. Dynamic shifts of visual receptive fields in cortical area MT by spatial attention. Nat. Neurosci. doi:10.1038/nn1748.
Womelsdorf, T., Anton-Erxleben, K., Treue, S., 2008. Receptive field shift and shrinkage in macaque middle temporal area through attentional gain modulation. J. Neurosci. 28, 8934–8944.
Yildirim, F., Carvalho, J., Cornelissen, F.W., 2018. A second-order orientation-contrast stimulus for population-receptive-field-based retinotopic mapping. Neuroimage 164, 183–193.